DOI: 10.19884/j.1672-5220.202503015

Underwater Recoverable Superhydrophobic Surface with Hierarchical Structure

TAN Zhimin[1], SHEN Hao[2], ZHAO Yiping[3], YANG Lili[1*], GE Dengteng[3]
1. State Key Laboratory of Advanced Fiber Materials, College of Materials Science and Engineering, Donghua University, Shanghai 201620, China
2. Institute of Functional Materials, Donghua University, Shanghai 201620, China
3. Institute for Engineering and Technology (Shanghai), Xinxing Cathay International Group, Shanghai 201403, China

Abstract: Underwater superhydrophobic surfaces (SHSs) are promising for drag reduction but are limited by the metastability of underwater air plastrons. Inspired by the replenishment mechanism of the water spider's air plastron, a recoverable SHS with a sparse micro-nano hierarchical structure was fabricated by obtaining a microcone array structure through laser etching and mold replication, followed by the chained nanoparticle deposition and fluorination treatment. The surface exhibited exceptional durability, sustaining 100 abrasion cycles (2 kPa) and 5.5 h water jetting (25 kPa). This is attributed to the microcone array, which protects the superhydrophobic nanoparticles under mechanical action. The hierarchical structure exhibited underwater aerophilicity, which enabled 34 cycles from fully wetting to superhydrophobicity. Rotational rheometric analysis revealed a drag reduction rate of 13.6%. Fluid dynamics simulations showed that the microstructure reduced wall shear stress, achieving a drag reduction rate of 14.2% at a flow velocity of 1 m/s and a wall-slip velocity of 0.15 m/s. This study provides design directions and theoretical foundations for the application of SHS in sustainable drag reduction.

Keywords: underwater; recoverable superhydrophobic surface; hierarchical structure; air plastron
CLC number: TB34 **Document code**: A
Article ID: 1672-5220(2026)02-0001-09

Open Science Identity (OSID)

0 Introduction

Drag reduction technologies have become critical in vessels, submarines, torpedoes and petroleum transportation[1-2], as frictional resistance constitutes approximately 50% and 60%–70% of the total drag for surface ships and submersibles, respectively[3-4]. The shipping sector, responsible for 80% of global trade, generates about 3% of anthropogenic greenhouse emissions[5]. Superhydrophobic surfaces (SHSs) have emerged as the most promising solution to drag reduction through air plastron formation at liquid-solid interfaces, where low-viscosity gas lubrication achieves 20%–30% drag reduction[6-8]. While current research has extensively characterized SHS drag reduction mechanisms, the metastability of air plastrons under hydrodynamic stresses remains insufficiently addressed. Plastron collapse induced by the flow velocity or pressure causes irreversible transitions to high-resistance wetted states[9]. Such failures significantly increase frictional resistance[10]. Therefore, the recoverability of SHSs is an essential requirement for achieving long-term drag reduction in underwater environments.

Enhancing the structural stability by improving the mechanical strength of material surfaces[11-13] constitutes a crucial strategy for effectively maintaining the integrity of the underwater air plastron. Underwater air plastron stabilization has been explored through hierarchical structures that enhance gas-liquid interface pinning via longitudinal ridges and patterned cavities[14], as well as through hybrid surfaces that combine low-adhesion superhydrophobic and high-adhesion hydrophobic regions[15-16]. These passive approaches inadequately address plastron metastability under working conditions. Active replenishment methods, including surface electrolysis[17], photolysis[18], photocatalysis[19] and H_2O_2 decomposition[20], require external energy/chemical inputs that restrict scalability. Aerophilic surfaces enabling spontaneous bubble spreading present sustainable alternatives[6-7], such as polydivinylbenzene nanofiber coatings. However, the recovery of the Cassie state from fully wetted surfaces remains underexplored. Sparse aerophilic nanoparticle structures demonstrate reversible wetted to superhydrophobic transitions[21]. However, insufficient plastron thickness limits the drag reduction efficiency based on the slip length theory and flow simulations[22-23]. SHSs with hydrodynamic drag reduction and autonomous air plastron recovery constitute an unresolved technical challenge.

In nature, water spiders utilize setal arrays to form

Received date: 2025-03-14
Foundation items: National Natural Science Foundation of China (Nos. 51973033 and 11774049)
* Correspondence should be addressed to YANG Lili, email: liliyang@dhu.edu.cn
Citation: TAN Z M, SHEN H, ZHAO Y P, et al. Underwater recoverable superhydrophobic surface with hierarchical structure[J]. *Journal of Donghua University (English Edition)*, 2026, 43(2): 1-9.

underwater air plastrons for respiration, which are periodically replenished at the water surface upon air plastron depletion. Inspired by this replenishment mechanism, an underwater recoverable superhydrophobic surface (URSS) featuring a bioinspired micro-nano hierarchical structure was designed. This study aims to develop a URSS with exceptional air plastron recovery and drag reduction capabilities. By designing a bioinspired architecture, this work sets out to address the challenge of air plastron instability on submerged SHSs and to establish a theoretical foundation for high-performance drag-reducing materials. The successful development of this technology is expected to hold broad application potential in naval engineering, submersible equipment, and microfluidic systems.

1 Materials and Methods

1.1 Materials

Tetraethyl orthosilicate (TEOS), *L*-arginine, anhydrous ethanol, acetone, sodium hydroxide (NaOH), hydrochloric acid (HCl) and 3-aminopropyltriethoxysilane (APTES) were purchased from Sinopharm Chemical Reagent Co., Ltd., China. Polydimethylsiloxane (PDMS, Sylgard 184) was obtained from the New Materials Division of Xinke, Dongguan, China. 1H, 1H, 2H, 2H-perfluorodecyltrichlorosilane (FDTS) was sourced from Shanghai Aladdin Biochemical Technology Co., Ltd., China.

1.2 Synthesis of URSS

1.2.1 Microcone array fabrication

A stainless steel substrate (3 cm × 3 cm × 3 mm) was micro-structured in ambient air by using a UV laser system (GQ-50, Chengdu Weishi Intelligent Creation Laser Equipment Co., Ltd., China). Periodic array patterns with conical apertures (a diameter of 100 μm, a height of 150 μm, and a pitch of 150 μm) were designed via CAD software. Laser processing was performed at a pulse frequency of 20 kHz, a scan speed of 500 mm/s and an output power of 15 W, with four repetitive scans applied to achieve the micro-structured substrate.

PDMS prepolymer and curing agents were mixed at a mass ratio of 10∶1, homogenized by 5 min stirring, and subjected to vacuum degassing for 10–20 min. The degassed PDMS solution was cast onto the micro-structured substrate surface, followed by thermal curing at 65 ℃ for 2 h. The cured PDMS film was peeled, trimmed, and ultrasonically cleaned in ethanol before drying for subsequent use.

1.2.2 Preparation of hierarchical structure

The micro-structured PDMS surface was subjected to oxygen plasma treatment for 10 min, followed by immersion in a 20 mmol/L APTES ethanol solution and reacted at 60 ℃ for 45 min. After ethanol rinsing, it was dried at 37 ℃. Chained nanoparticles (CNPs) were prepared according to the method reported in Ref. [18]. It was dispersed in deionized water at mass fractions of 0.2%, 0.4% and 0.6%, and ultrasonicated for 30 min at pH = 6. The pre-treated micro-structured PDMS surface was then immersed in the CNP solution for 1 h, and subsequently dried. The corresponding samples were named 0.2%CNPs, 0.4%CNPs, and 0.6%CNPs, respectively.

1.2.3 Fluorination treatment

The PDMS with a hierarchical structure was subjected to oxygen plasma treatment for 10 min to promote hydroxylation, followed by exposure to a vacuum chamber containing 100 μL FDTS for 30 min to undergo chemical vapor deposition, thereby achieving superhydrophobicity. After heating at 65 ℃ for 10 min, the sample was sequentially rinsed with acetone and deionized water to obtain the final product. The schematic of the preparation process is shown in Fig. 1.

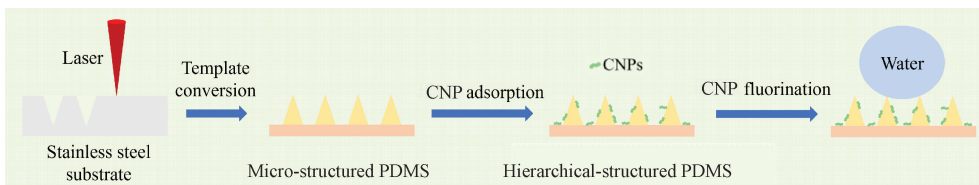

Fig. 1 Schematic diagram for preparation of URSS with hierarchical structure

1.3 Characterization methods

Surface morphology was characterized by a scanning electron microscope (S-4800, Hitachi, Japan). The water contact angle (CA) and sliding angle (SA) were measured via a contact angle goniometer (SL200KB, Kino, USA). Bubble contact angles were measured via the sessile drop method in water, captured by a high-speed camera (Chronos 1.4, Kron, USA). Mechanical durability was carried out by using a reciprocating friction tester (ZJ-339-GSR, Shenzhen Zhijia Instrument Co., Ltd., China) with 1 500-grit sandpaper under 2 kPa loading. The water jetting experiment was conducted by mounting specimens on 45° inclined plates 5 cm from a 3 mm nozzle at a pressure of 25 kPa. Bubble-surface interactions were quantified via an atomic force microscope (Multi Mode8, Bruker, USA) coupled with Nikon Ti-U inverted optics to confirm aerophilicity. Ethanol-induced wetting failure specimens underwent recovery cycling via air bubble introduction, with CA/SA monitored until performance degradation. The torque M was measured via a rotational rheometer (MCR302, Anton Paar, Austria) by using a 25 mm plate rotor, with

a shear rate $\dot{\gamma}$ of $40-100\ s^{-1}$. The slip length on the structured surface b and drag reduction rate r were computationally derived from the torque as follows:

$$b = D_h \times \left(\frac{\pi R^3 \mu \dot{\gamma}}{2M} - 1\right), \quad (1)$$

$$r = (b' - b)/b' \times 100\%, \quad (2)$$

where R, D_h, μ and b' indicate the rotor radius, the gap between the rotor and the sample, the fluid viscosity and the slip length on the smooth surface, respectively.

1.4 Numerical simulation

Numerical simulations of hydrodynamic drag reduction were performed by using ANSYS Fluent 17.0, with computational geometry constructed in AutoCAD 2023. A three-dimensional domain (300 mm × 80 mm × 50 mm) contained 5 × 4 periodic microstructures (5 mm in diameter, and 7.5 mm in height and pitch) and was positioned 100 mm downstream from the inlet to minimize entrance effects. The multiphase flow was resolved through the volume of fluid (VOF) method with the SIMPLEC pressure-velocity coupling algorithm and standard k-ε turbulence model by using scalable wall functions. A second-order upwind scheme was adopted for spatial discretization, with the convergence criteria set to residuals below 1×10^{-2} (maximum 1 000 iterations). Boundary conditions included a mainstream velocity of 1 m/s and a wall-slip velocity of 0–0.15 m/s. The drag reduction rate D_R was calculated via

$$D_R = (\tau_0 - \tau)/\tau_0 \times 100\%, \quad (3)$$

where τ_0 and τ represent the shear stresses on the smooth and micro-structured surfaces, respectively.

2 Results and Discussion

2.1 Characterization of URSS

The microstructural characteristics and performance of URSS are presented in Fig. 2. The low-resolution scanning electron microscopy (SEM) image (Fig. 2(a)) reveals periodic circular pore arrays (a diameter of 100 μm, and a pitch of 150 μm). The high-resolution SEM image (Fig. 2(b)) demonstrates densely aligned CNPs (about 200 nm in length, about 50 nm in diameter), establishing essential structural support for air plastron stabilization. Cross-sectional microscopy image (Fig. 2(c)) confirms a microstructure height of 150 μm, a geometric configuration that enhances air entrapment and interfacial stability. The water CA on this surface reaches 151° (Fig. 2(d)), with a water SA of 7°, exhibiting superhydrophobic properties.

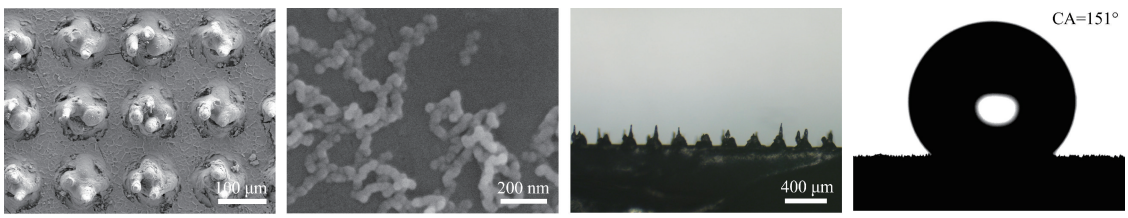

Fig. 2 Microstructural characteristics and performance of URSS: (a) low-resolution SEM image; (b) high-resolution SEM image; (c) cross-sectional microscopy image; (d) water CA measurement image

2.1.1 Mechanical durability of URSS

Mechanical durability of URSS is recognized as a critical performance index for underwater applications. Specimens were evaluated through abrasive cycling (2 kPa) and hydrodynamic impact testing (25 kPa). The abrasion test schematic and water jetting test schematic are shown in Figs. 3(a) and 3(b), respectively. Figure 3(c) shows that the sample surface with the hierarchical structure withstands 100 abrasion cycles, tripling the endurance of the unitary nanostructure (30 cycles). Under the hydrodynamic stress, the hierarchical structure maintains stable performance for 5.5 h vs. 2.0 h for the unitary nanostructure (Fig. 3(d)). This performance disparity is attributed to stress-dissipative networks formed by interlocked microstructure in a hierarchical-structure system, effectively redistributing shear stresses to protect surface nanoparticles. The study confirms that micro-nano hierarchical structures enhance the interfacial bonding strength compared to unitary nanostructures, providing critical insights for underwater environmental applications. The microcone array tips preferentially undergo deformation due to stress concentration effects (inherent to geometric tip characteristics), as demonstrated in Figs. 3(e) and 3(f). The interstitial regions between microcones maintain relatively lower damage levels owing to structural support from adjacent features. Although surface-attached CNPs experience fracture or detachment under frictional shear forces, the physical confinement effect exerted by the microcone architecture partially mitigates extensive nanoparticle detachment.

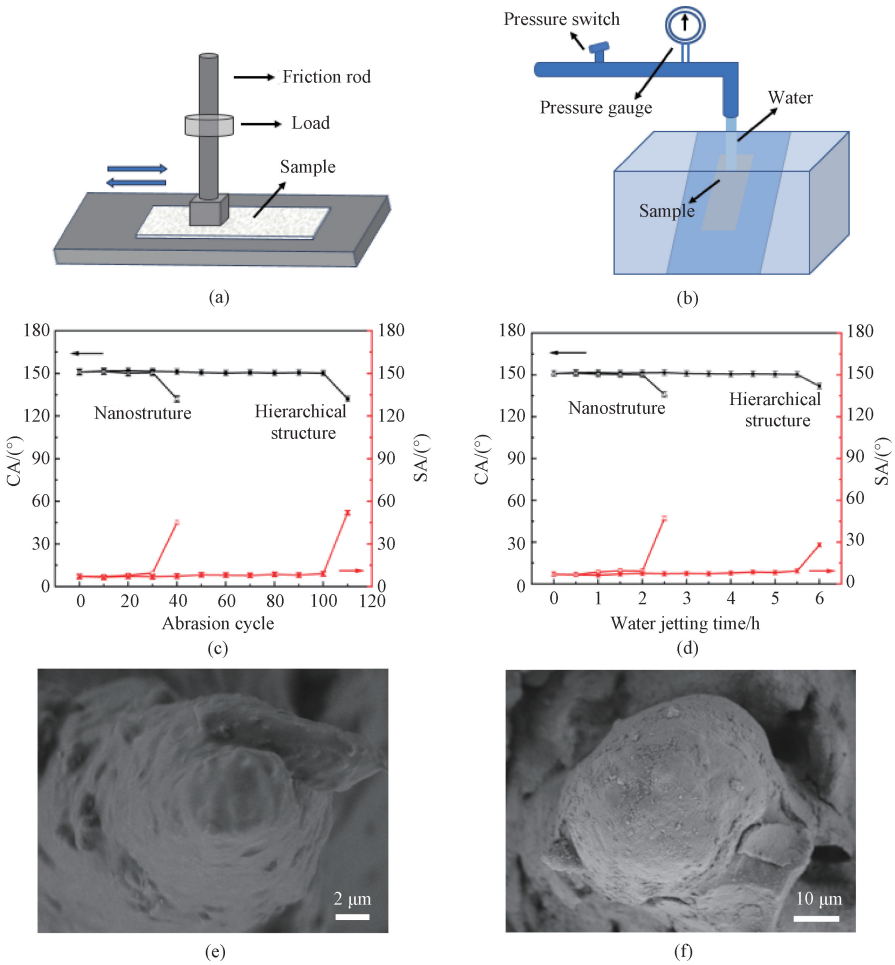

Fig. 3 Mechanical durability tests: (a) abrasion test schematic; (b) water jetting test schematic; (c) CA and SA vs. abrasion cycle; (d) CA and SA vs. water jetting time; (e) SEM image of URSS after 100 abrasion cycles at 2 kPa; (f) SEM image of URSS after water jetting for 5.5 h at 25 kPa

2.1.2 Aerophilic performance of URSS

Bubble-surface interaction mechanisms were quantitatively investigated through atomic force microscopy (AFM) bubble probe technology (Fig. 4(a)). The ethanol-pretreated sample was submerged. A bubble probe was then vertically approached to the sample by controlled piezo displacement. Force vs. piezo displacement curves revealed initial repulsion at a piezo displacement of 3 μm progressing to a maximum adhesion of 20 nN at contact (Fig. 4(b)), and a final bubble detachment force of 37 nN upon probe retraction at a piezo displacement of 9 μm (Fig. 4(c)). Synergistic effects between low steric hindrance at microstructure apices and surface nanoparticles were identified as critical stabilization mechanisms. This discovery elucidates surface-directed bubble behavior regulation, providing experimental and theoretical foundations for optimizing air plastron stability in submerged superhydrophobic systems.

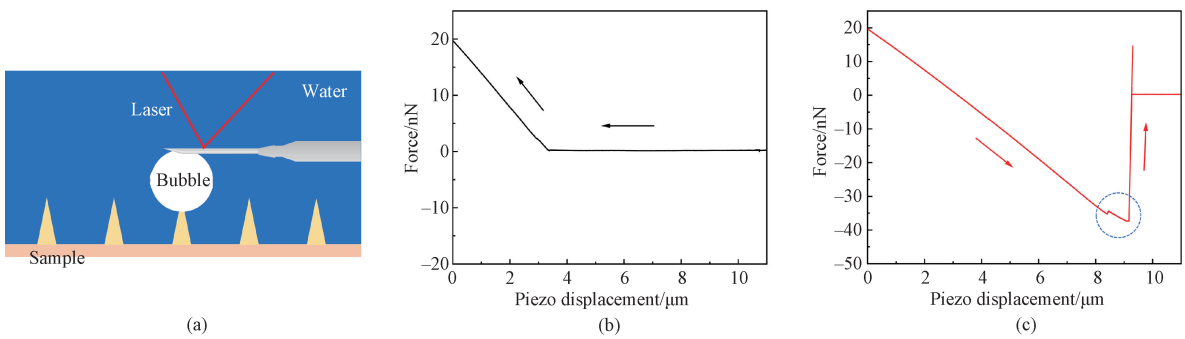

Fig. 4 Interaction force tests and results: (a) testing diagram; (b) attachment curve; (c) pickup curve

2.1.3 Underwater recoverable performance of URSS

Bubble penetration dynamics in microcavities were modeled based on Boyle's law. The theory of recoverable superhydrophobicity can be represented by the relationship between the ratio of the bubble spreading depth h to the structure height H and the ratio of H to the structure pitch L[21]:

$$\frac{h}{H}=\frac{P_0}{P_L+8\pi(D+d)\cdot\gamma\cdot\cos\theta/[16L^2-\pi(D+d)^2]}-\frac{2\sqrt{2}-(d+D)/L}{12\cos^3\theta}\cdot\frac{1}{H/L}(2-3\sin\theta_{adv}+\sin^3\theta_{adv}),\quad(4)$$

where P_0 and P_L are the bubble pressure and hydrostatic pressure, respectively; d, D, γ, θ, and θ_{adv} represent the apical diameter, basal diameter, surface tension of water, CA on the fluorinated flat and smooth surface, and CA on the conical structure, respectively.

Here, initial parameters are set to $P_0=101.3$ kPa, $P_L=180$ kPa (a water depth of 18 m), $d=0$, $D=L=150$ μm, $\gamma=0.072$ N/m (at 25 ℃), $\theta=110°$, and $\theta_{adv}=125°$. Figure 5(a) shows the numerical simulation of the relationship of h/H and H/L. When $H/L<0.95$, $h/H=1$, which indicates that the bubbles displace water between microstructures, ultimately filling their base. When $H/L>0.95$, $h/H<1$, which indicates that the bubbles fail to reach the base of microstructures, preventing full recovery from the wetted state. The designed microstructures, with $H=L=150$ μm (i.e., $H/L=1$), have a ratio close to the theoretical critical ratio (0.95), enabling surface recovery from a fully wetted state.

Bubble recoverability was validated through ethanol-induced wetting followed by systematic bubble replenishment. The submerged sample was subjected to bubble injection. The bubble CA monitoring reveals a rapid reduction of about 50° within 10 s (Fig. 5(b)), confirming aerophilicity-driven lateral spreading. As shown in Fig. 5(c), the released bubble first ascends to contact the sample surface, undergoes deformation-rebound, and then initiates lateral expansion. Continuous bubble supply induces coalescence into continuous air plastrons, achieving full Cassie-Baxter state recovery within 11.6 s. Contact with nanoparticles at microstructure apexes initiates lateral bubble expansion through understructure gaps, displacing trapped water to ultimately restore the surface air plastron. This demonstrates micro-nano hierarchical structural regulation of bubble dynamics.

Cyclic wetting-recovery testing demonstrates the sustained performance over 34 cycles, maintaining CA more than 150° and SA less than 10° (Fig. 5(d)). The findings validate the practical reliability of underwater recoverability, offering critical experimental guidance for superhydrophobic material design. Furthermore, the results establish theoretical frameworks for engineering applications such as ship drag reduction and microfluidic systems.

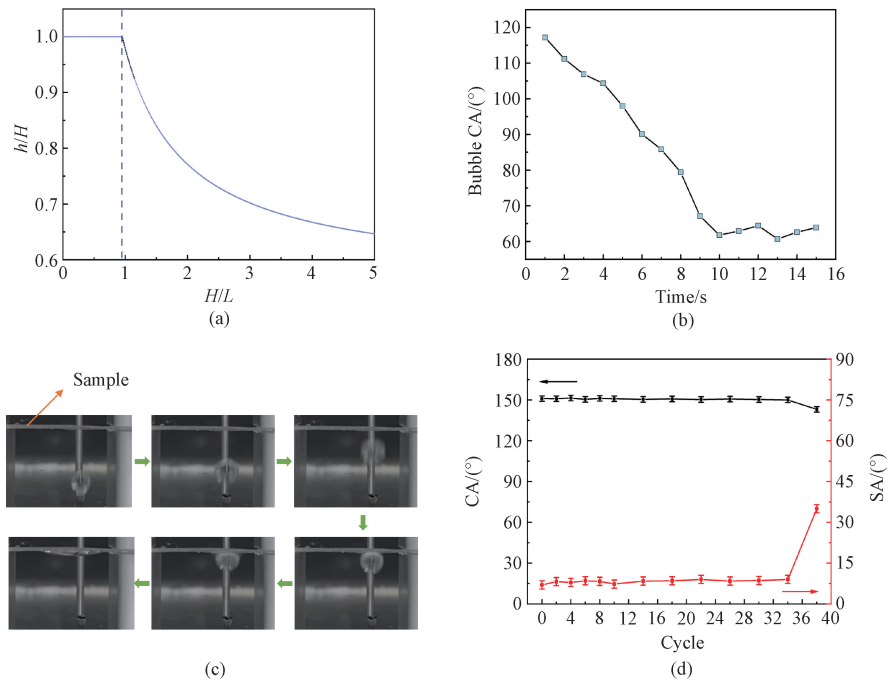

Fig. 5 Underwater recoverable performance: (a) theoretical modeling of bubble expansion process; (b) contact angles for bubble on wetted sample; (c) process of surface recovery by bubble replenishment; (d) cyclic performance of wetting recovery performance

2.2 Drag reduction performance of URSS

Hydrodynamic drag reduction performance was evaluated through a designed free-falling test system. The apparatus comprised a transparent cylindrical tank (a

diameter of 30 cm, a height of 120 cm) filled with deionized water to a depth of 110 cm. Two identical specimens were symmetrically mounted on a stainless-steel block, simultaneously released with a control group at the water surface. High-speed videography (4 489 frames per second) captured descent trajectories, with bottom arrival time differentials recorded. The falling distance was determined by the position of the specimen's top. Triplicate trials (Table 1) demonstrate a reduction of 0.16 s in the falling time for specimen-equipped stainless-steel blocks, corresponding to effective interfacial drag reduction via air plastron stabilization by the micro-nano hierarchical structure. The result validates practical hydrodynamic efficiency while providing critical experimental benchmarks for marine engineering applications.

Table 1 Free-falling test results

Sample	Average falling time/s
Blank stainless steel	2.67
Stainless steel with URSS pasted on both sides	2.51

The drag reduction performance and its modulation mechanisms were systematically investigated through the rotational rheometric analysis of CNP concentration effects. The testing device is shown in Fig. 6(a). Compared to 0.2%CNPs and 0.6%CNPs within a shear rate range of 40 to 100 s^{-1}, 0.4%CNPs exhibits superior torque and drag reduction rate, as shown in Figs. 6(b) and 6(c), respectively. Notably, 0.4%CNPs achieves a drag reduction rate of 13.6% at a shear rate of 40 s^{-1}. Performance variation arises from concentration-modulated surface structural modifications. Excessive CNP loading (a mass fraction of 0.6%) induces nanoparticle aggregation and flow-induced detachment, thereby compromising superhydrophobic integrity, while insufficient CNP loading (a mass fraction of 0.2%) results in inadequate surface coverage for microstructure stabilization. The 0.4% formulation achieves an optimal equilibrium between the surface packing density and interfacial adhesion strength, enabling enhanced hydrodynamic performance. The finding elucidates the concentration-modulated drag reduction mechanism while establishing fundamental design principles for engineering highly performant superhydrophobic surfaces in fluid dynamics and microfluidic applications.

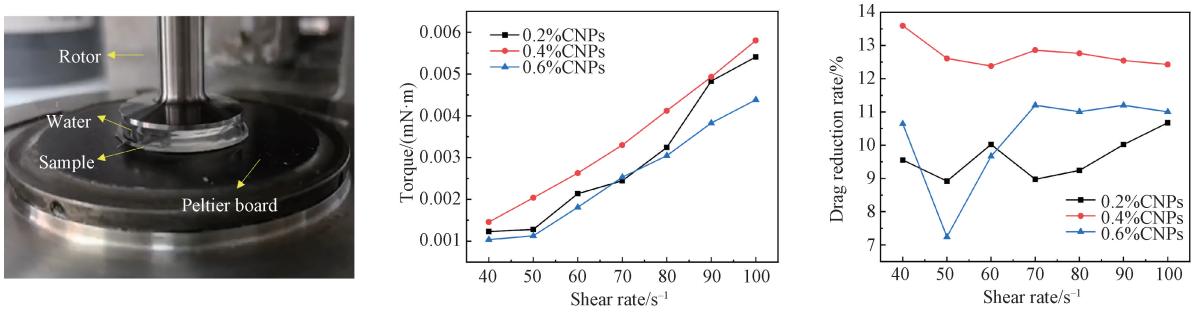

(a) (b) (c)

Fig. 6 Rotational rheometer measurements and results: (a) image of testing device; (b) diagram of torque vs. shear rate; (c) diagram of drag reduction rate vs. shear rate

2.3 Numerical simulation of drag reduction on URSS

Numerical simulations were conducted to evaluate gas-liquid interfacial flow dynamics and their drag reduction mechanisms through velocity distribution analysis of microstructure surfaces (Fig. 7). Non-superhydrophobic surfaces were initially modeled by using no-slip boundary conditions, revealing lower flow velocities in microstructural gaps than those in planar regions (Figs. 7(a) and 7(b)), corresponding to a drag reduction rate of 10.5% (calculated from the velocity distribution data). Subsequent implementation of wall-slip conditions (0.15 m/s, the dashed in Fig. 7(c)) for superhydrophobic surfaces generated low-velocity zones near microstructure walls, with minimized shear stress in gaps, elevating the drag reduction rate to 14.2% (also calculated from the velocity distribution data). This simulated value aligned with rotational rheometer measurements (13.6% maximum reduction), confirming experimental-simulative consistency. The effectiveness of the micro-nano hierarchical structure in drag reduction optimization was thereby confirmed. A fundamental correlation between microstructure geometry and gas-liquid interfacial flow dynamics was established, advancing design principles for enhanced superhydrophobic materials.

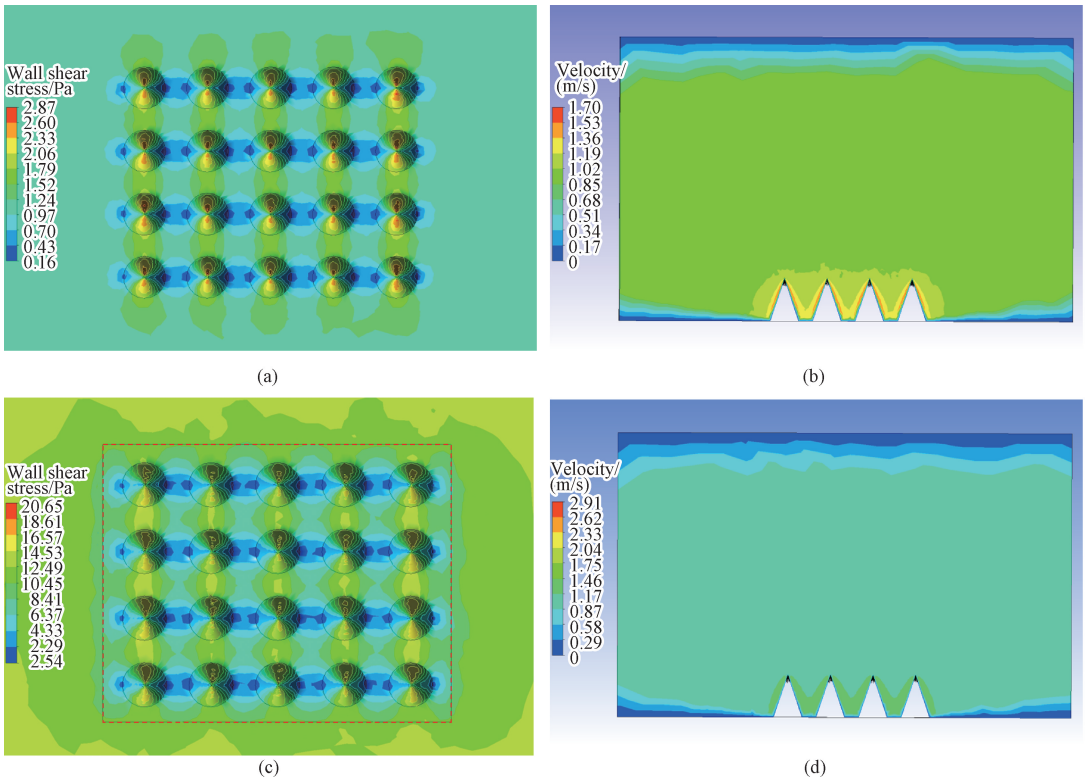

Fig. 7 Drag reduction numerical simulation: (a) top view without wall-slip; (b) cross-sectional view without wall-slip; (c) top view with wall-slip; (d) cross-sectional view with wall-slip

3 Conclusions

In summary, a biomimetic superhydrophobic surface with micro-nano hierarchical architecture was fabricated through laser ablation and PDMS replication, chained nanoparticle deposition, and fluorination treatment. Mechanical durability was experimentally validated through 100-cycle bidirectional abrasion (2 kPa) and 5.5 h hydrodynamic erosion (25 kPa), achieved through microstructure-enabled nanoparticle protection. Plastron regeneration (11.6 s bubble replenishment) with 34-cycle durability was demonstrated. Rheometric measurements confirmed a drag reduction of 13.6%, and numerical simulations showed a resistance decrease of 14.2% (a flow velocity of 1 m/s, and a slip velocity of 0.15 m/s). Microstructural analysis revealed wall shear stress reduction through velocity gradient attenuation and boundary layer optimization. The synergistic mechanism of gas transport and interfacial stability regulation was verified via the hierarchical architecture. Compared with conventional designs, microcone-nanostructure hybridization enhanced both air plastron recoverability and hydrodynamic performance. Limitations persist in high-velocity flow stabilization and multiphase fluid interactions. This study establishes theoretical and technical foundations for high-performance superhydrophobic materials, demonstrating promising applications in marine drag reduction and microfluidic systems.

References

[1] BAI X, GOU X D, ZHANG J L, et al. A review of smart superwetting surfaces based on shape-memory micro/nanostructures[J]. *Small*, 2023, 19(15): 2206463.

[2] WANG X L, HASSAN A, BOUDAOUD H, et al. A review on 3D printing of bioinspired hydrophobic materials: oil-water separation, water harvesting, and diverse applications[J]. *Advanced Composites and Hybrid Materials*, 2023, 6(5): 170.

[3] ZHANG J S, GABILLET C, BILLARD J Y. Experimental study of the bubbly drag reduction in the recovery region of a separated turbulent boundary layer[J]. *International Journal of Multiphase Flow*, 2021, 142: 103697.

[4] GU Y Q, ZHAO G, ZHENG J X, et al. Experimental and numerical investigation on drag reduction of non-smooth bionic jet surface[J]. *Ocean Engineering*, 2014, 81: 50-57.

[5] BAUMANN J. Shifting to sustainable shipping: actors and power shifts in shipping emissions in the IMO[J]. *Sustainability*, 2023, 15(17): 12742.

[6] ELBING B R, MÄKIHARJU S, WIGGINS A, et al. On the scaling of air layer drag reduction [J]. *Journal of Fluid Mechanics*, 2013, 717: 484-513.

[7] ELBING B R, WINKEL E S, LAY K A, et al. Bubble-induced skin-friction drag reduction and the abrupt transition to air-layer drag reduction [J]. *Journal of Fluid Mechanics*, 2008, 612: 201-236.

[8] MURAI Y, OIWA H, TAKEDA Y. Frictional drag reduction in bubbly Couette-Taylor flow [J]. *Physics of Fluids*, 2008, 20(3): 034101.

[9] DUAN H L. Underwater superhydrophobicity: fundamentals and applications [J]. *Procedia IUTAM*, 2017, 20: 128-135.

[10] KARATAY E, HAASE A S, VISSER C W, et al. Control of slippage with tunable bubble mattresses [J]. *Proceedings of the National Academy of Sciences of the United States of America*, 2013, 110(21): 8422-8426.

[11] XIAO J X, ZHAN B B, HE M K, et al. Mechanically robust and thermal insulating nanofiber elastomer for hydrophobic, corrosion-resistant, and flexible multifunctional electromagnetic wave absorbers [J]. *Advanced Functional Materials*, 2025, 35(14): 2419266.

[12] TANG L, TANG Y S, ZHANG J L, et al. High-strength super-hydrophobic double-layered PBO nanofiber-polytetrafluoroethylene nanocomposite paper for high-performance wave-transparent applications [J]. *Science Bulletin*, 2022, 67(21): 2196-2207.

[13] DING F M, GUO Y L, WANG Q M, et al. Review of antifouling finishing of textiles: theme, evolution and fabrication methods [J]. *Journal of Donghua University (English Edition)*, 2024, 41(6): 616-629.

[14] CHEN Y M, HU Y, ZHANG L W. Effective underwater drag reduction: a butterfly wing scale-inspired superhydrophobic surface [J]. *ACS Applied Materials & Interfaces*, 2024, 16(20): 26954-26964.

[15] HU H B, WEN J, BAO L Y, et al. Significant and stable drag reduction with air rings confined by alternated superhydrophobic and hydrophilic strips [J]. *Science Advances*, 2017, 3(9): e1603288.

[16] YAO X, YANG Y, LI G Q, et al. Enhancing gas film stability by alternating superhydrophobic and hydrophobic surfaces for stable drag reduction [J]. *Applied Physics Letters*, 2024, 124(17): 171603.

[17] LLOYD B P, BARTLETT P N, WOOD R J K. Active gas replenishment and sensing of the wetting state in a submerged superhydrophobic surface [J]. *Soft Matter*, 2017, 13(7): 1413-1419.

[18] LEE J H, YONG K J. Combining the lotus leaf effect with artificial photosynthesis: regeneration of underwater superhydrophobicity of hierarchical ZnO/Si surfaces by solar water splitting [J]. *NPG Asia Materials*, 2015, 7(7): e201.

[19] AEBISHER D, BARTUSIK D, LIU Y, et al. Superhydrophobic photosensitizers. Mechanistic studies of $^1O_2$ generation in the plastron and solid/liquid droplet interface [J]. *Journal of the American Chemical Society*, 2013, 135(50): 18990-18998.

[20] PANCHANATHAN D, RAJAPPAN A, VARANASI K K, et al. Plastron regeneration on submerged superhydrophobic surfaces using in situ gas generation by chemical reaction [J]. *ACS Applied Materials & Interfaces*, 2018, 10(39): 33684-33692.

[21] ZHAO Y P, XU Z, GONG L, et al. Recoverable underwater superhydrophobicity from a fully wetted state via dynamic air spreading [J]. *iScience*, 2021, 24(12): 103427.

[22] VORONOV R S, PAPAVASSILIOU D V, LEE L L. Slip length and contact angle over hydrophobic surfaces [J]. *Chemical Physics Letters*, 2007, 441(4/5/6): 273-276.

[23] ZHANG R L, DI Q F, WANG X L, et al. Numerical study of the relationship between apparent slip length and contact angle by lattice Boltzmann method [J]. *Journal of Hydrodynamics*, 2012, 24(4): 535-540.

具有分级结构的水下可恢复超疏水表面

谭志敏[1]，沈　浩[2]，赵一平[3]，杨丽丽[1*]，葛邓腾[3]

1. 东华大学 先进纤维材料全国重点实验室 材料科学与工程学院，上海 201620
2. 东华大学 功能材料研究中心，上海 201620
3. 新兴际华（上海）工程科技研究院有限公司，上海 201403

摘　要：水下超疏水表面在减阻领域具有广阔前景，但其应用受限于表面气盾的水下不稳定性。受水蜘蛛气盾补充机制启发，首先通过激光刻蚀和翻模法获得微锥阵列结构，然后进行链状纳米粒子沉积和氟化处理，制备出具有稀疏微-纳分级结构的可恢复超疏水表面。该超疏水表面表现出优异的耐久性，可承受 100 次摩擦循环(2 kPa)，5.5 h 水流冲击(25 kPa)。这归因于微锥阵列，其在机械作用下保护了超疏水纳米粒子。该分级结构具有水下亲气性，可实现 34 次从完全润湿到超疏水状态的循环转变。旋转流变试验计算得知该表面减阻率达 13.6%。流体动力学模拟表明该微结构降低了表面的壁面剪切力，在水流速度为 1 m/s、壁面滑移速度为 0.15 m/s 时，减阻率达 14.2%。该研究为超疏水表面长效可持续减阻应用提供了理论依据和设计方向。

关键词：水下；可恢复超疏水表面；分级结构；气盾